High-resolution electron microscopy observation of the fine structure of Cu-Zn-Al martensites

1992 J. Phys.: Condens. Matter 4 2397

(http://iopscience.iop.org/0953-8984/4/10/006)

J. Phys.: Condens. Matter 4 (1992) 2397–2403. Printed in the UK

High-resolution electron microscopy observation of the fine structure of Cu–Zn–Al martensites

R Wang†, C Luo†, J Gui†, Q Ren† and J Chen‡

† Laboratory of Material Physics, Department of Physics, Wuhan University, 430072 Wuhan, People's Republic of China

‡ Laboratory of Solid State Microstructures, Nanjing University, 210008 Nanjing, People's Republic of China

Received 7 October 1991

Abstract. The fine structure of martensites in step-quenched Cu–17.4 at.% Zn–13.0 at.% Al alloy has been observed using high-resolution electron microscopy. It has been found that, besides the $18R_1$ martensite occurring most frequently, there exist also 6R and 2H martensites in local regions. Stacking faults, extended dislocations with Burgers vector $\frac{1}{3}[210]_{6R}$ and basal plane twins have also been observed in 6R martensite. The planarity and coherency of the $(2, 0, 20)_{18R_1}$ A–D twin boundary of $18R_1$ martensite are much less than those of the $(12\bar{8})_{18R_1}$ A–C twin boundary. Edge dislocations, whose Burgers vector has a component in the $[001]_{18R_1}$ direction, have been observed near the $(2, 0, 20)_{18R_1}$ boundary.

1. Introduction

The formation of multiple martensite variants after martensitic transformation by cooling and the ease of the migration of the intervariant interfaces and the parent–martensite interfaces play a key role in the shape memory effect (SME) (see, e.g. the review article in [1]). Therefore, much attention has been paid to the observation of the fine structure of the interfaces in shape memory alloys (SMAs).

Sinclair and Mohamed [2] observed for the first time the parent–martensite interface in the SMA NiTi by using the lattice-imaging technique of high-resolution electron microscopy (HREM) and found that the parent and martensite phases are fully coherent. Fukamachi and Kajiwara [3] observed the intervariant $(11\bar{4})_{9R}$ interface of the 9R martensite in Cu–33.40 at.% Zn–1.58 at.% Si SMA also by using the lattice-imaging technique of HREM. They showed that the boundary is coherent except at the places where stacking faults exist. Knowles [4–6] and Knowles *et al* [7] observed the structure of the parent–martensite interface, transformation twin and intervariant interfaces in Ni–Ti, Ti–5 wt% Mn and Au–47.5 at.% Cd alloys using HREM. They showed that the parent–martensite interface in the Ti–5 wt% Mn alloy can be effectively considered to be coherent, that there is evidence for the step and ledge structure of twin interfaces in Ni–Ti, Ti–5 wt% Mn and Au–47.5 at.% Cd alloys. At the same time, Cook *et al* [8, 9], Stobbs [10] and Adachi and Perkins [11] observed both $(12\bar{8})_{18R_1} = (11\bar{4})_{9R}$ and $(2, 0, 20)_{18R_1} = (2, 0, 10)_{9R}$ intervariant boundaries of the Cu–Zn–Al martensite by using HREM. They found that the A–C boundary is a straight coherent twin boundary

0953-8984/92/042397 + 07 $04.50

matching exactly the $(12\bar{8})_{18R_1} = (11\bar{4})_{9R}$ planes, and the A–D boundary, although generally planar and nearly parallel with $(2, 0, 20)_{18R_1} = (2, 0, 10)_{9R}$ plane, has a tendency to wander and form curved segments. Recently, Lovey and co-workers [12–14] discussed the influence of crystal orientation on the HREM image and observed the $(12\bar{1})_{2H}$-type twin interface of 2H martensite and $(12\bar{8})_{18R_1}$-type twin interface of $18R_1$ martensite in Cu–Al alloys and the parent–martensite interface in Cu–Zn–Al alloy. They found that these boundaries are quite coherent in spite of the existence of stacking faults in martensites. Moreover, the so-called parent–martensite interfacial dislocations with Burgers vector $\frac{1}{3}[001]$, as reported by Tadaki *et al* [15] in Cu–Al–Ni alloys studied by using conventional transmission electron microscopy (TEM), were not observed.

According to the phenomenological theory of the martensitic transformation, an appropriate basal plane stacking fault density in 9R or $18R_1$ martensite is needed to obtain an undistorted habit plane (see, e.g., [1, 16]). HREM observations of stacking faults in 9R and $18R_1$ martensites [3, 9, 10, 12, 16–18] revealed the existence of the face-centred cubic (FCC) (α-type) and the hexagonal (β-type) stacking faults and the agreement between the observed stacking fault densities and those needed from the phenomenological calculations. It was found that the stabilized alloy possesses a tendency to form cubic-type stacking faults [9, 10]. Neither the simple shear-type fault nor the twin-type fault [19] was identified positively by HREM [9, 10, 16]. Moreover, the nature of the so-called type I defect discovered by Andrade *et al* [20] was identified to be boundaries between two differently stacked martensite parts [12, 17] or a stacking fault plane [11].

The crystal structures of martensites in β Hume–Rothery alloys are long-period stacking-order structures [1]. The Cu–Zn–Al martensites are 9R (or $18R_1$) type when formed by cooling and 9R (or $18R_1$) and 3R (or 6R) types induced by an external stress [1, 21]. It is expected that martensites other than type 9R (or $18R_1$) may exist in quenched Cu–Zn–Al alloys because of the polytypism of the long-period stacking-order structure and the possible thermal and transformation stresses, at least in local regions of a specimen. Indeed, Wang *et al* [22] found 12R, 6R and 2H martensites besides $18R_1$ martensite in quenched Cu–Zn–Al alloys mainly by using the selected-area electron diffraction technique.

In the present work we have observed the fine structure of the quenched Cu–17.4 at.% Zn–13.0 at.% Al martensite using HREM. The fine structures studied are (1) the structure types of the martensites in local regions, (2) twin, stacking fault and extended dislocations in 6R martensite and (3) $(2, 0, 20)_{18R_1}$ intervariant boundaries in $18R_1$ martensite.

2. Experimental method

Cu–17.4 at.% Zn–13.0 at.% Al SMA was melted using raw materials of industrial purity. Samples were solid solution treated at 1073 K for 5 min, quenched into an oil bath at 433 K for 4 min and then quenched into cold water. The transition temperatures of such samples are $M_s = 388$ K, $M_f = 325$ K, $A_s = 349$ K and $A_f = 404$ K. TEM foils were prepared from plate specimen first by chemical thinning at room temperature in a solution of 1:4:5 $HCl:HNO_3:H_3PO_4$ and then by twin-jet electropolishing in a D2 solution at room temperature. HREM observation has been conducted using a JEOL 4000EX electron microscope equipped with a top-entry goniometer stage and operated at 400 kV. Although the most appropriate orientation for observing the basal plane

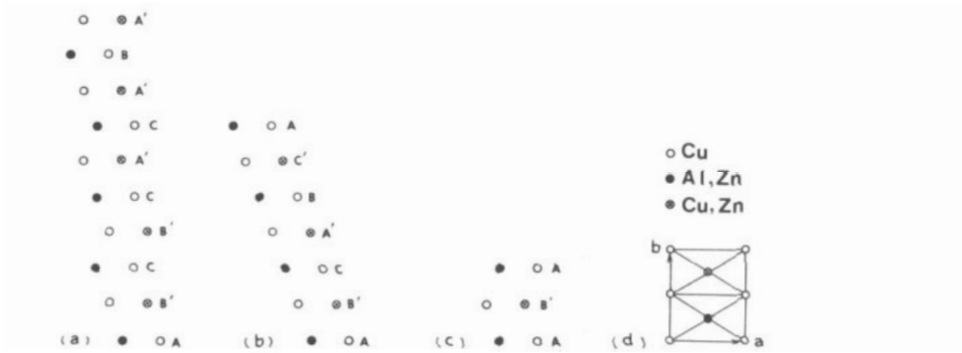

Figure 1. Martensite structures projected along [010] direction: (*a*) $18R_1$; (*b*) 6R; (*c*) 2H; (*d*) basal plane.

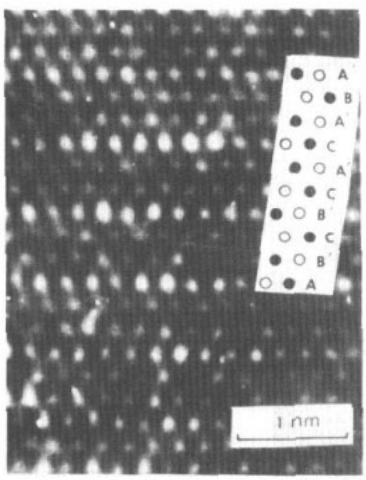

Figure 2. HREM image along the [010] zone axis showing the $18R_1$ martensite in step-quenched Cu–17.4 at.% Zn–13.0 at.% Al alloy.

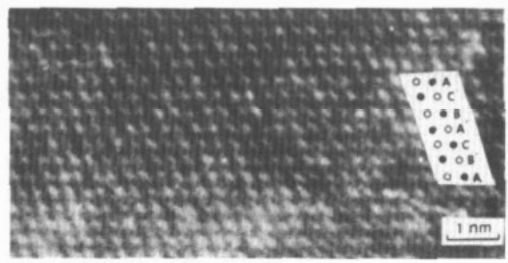

Figure 3. HREM image along the [010] zone axis showing a local 6R martensite in step-quenched Cu–17.4 at.% Zn–13.0 at.% Al alloy.

stacking sequence of the long-period stacking order structure is $[2\bar{1}0]_{18R_1}$ or $[210]_{18R_1}$ zones in the $18R_1$ martensite coordinate system [18] an $[010]_{18R_1}$ zone has been used in the present work for studying the fine structure of the $(2, 0, 20)_{18R_1}$ intervariant interface.

3. Results and discussion

3.1. Polytypism of the long-period stacking order martensite

Figures 1(*a*), (*b*) and (*c*) show martensite structures of $18R_1$, 6R and 2H types, respectively, transformed from the $D0_3$ ordered parent phase and projected along the [010] direction with the basal plane shown in figure 1(*d*). Most of the HREM image consists of a white dot pattern as shown in figure 2 which corresponds to a 9R- or a $18R_1$-type

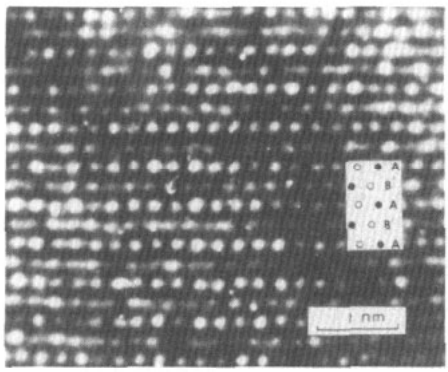

Figure 4. HREM image along the [010] zone axis showing a local 2H martensite in step-quenched Cu–17.4 at.% Zn–13.0 at.% Al alloy.

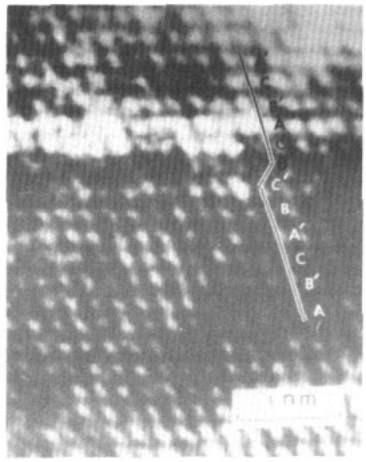

Figure 5. HREM image along the [010] zone axis of the 6R martensite in step-quenched Cu–17.4 at.% Zn–13.0 at.% Al alloy, showing a stacking fault.

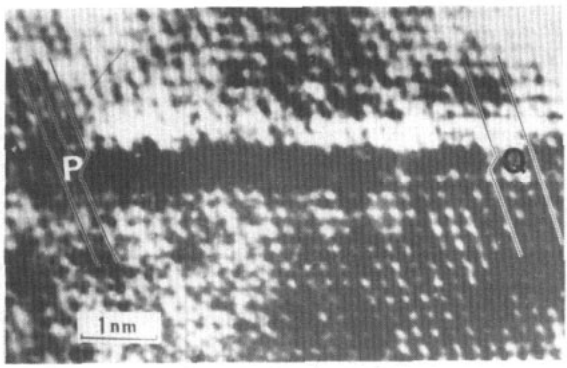

Figure 6. HREM image along the [010] zone axis of the 6R martensite in step-quenched Cu–17.4 at.% Zn–13.0 at.% Al alloy, showing an extended dislocation PQ with Burgers vector $\frac{1}{6}[210]$.

structure (figure 1(*a*)). The identification of the $18R_1$-type rather than the 9R-type structure was obtained by electron diffraction technique [22] along $[1\bar{1}0]$, $[2\bar{1}0]$ and [100] zone axes.

In some local regions, 6R-type martensite (figure 3) and 2H-type martensite (figure 4) have been observed. These HREM photographs are complementary to the electron diffraction identification of these martensites in quenched Cu–Zn–Al alloys as described in [11, 22]. Our observation is in good agreement with Suzuki's [23] numerical study. Suzuki found HCP (2H), FCC (3R or 6R) and 9R (or $18R_1$) structures obtained as a result of the time development of the transverse lattice waves with different parameters, respectively.

The 6R and 2H structure types possess an intimate connection with the stacking fault in $18R_1$ structure. As shown by Lovey *et al* [18], each β-type stacking fault creates locally

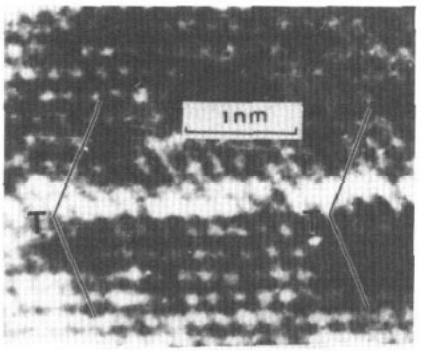

Figure 7. HREM image along the [010] zone axis of the 6R martensite in step-quenched Cu–17.4 at.% Zn–13.0 at.% Al alloy, showing a basal plane twin TT.

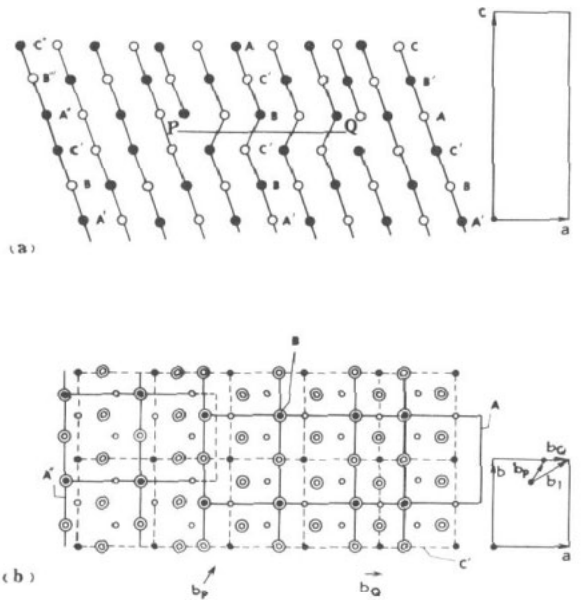

Figure 8. Schematic diagrams of the extended dislocation PQ in 6R martensite showing (*a*) a [010] projection and (*b*) the arrangement of atoms in two adjacent (001) planes: •, Al in the plane of the diagram; ○, Cu in the plane of the diagram; ⊙, Al in adjacent upper plane; ◎, Cu in adjacent upper plane.

a six-layer 2H structure. On the other hand, the elimination of the reverse stacking sequence in $18R_1$ martensite results in a local 6R structure.

3.2. Fine structures in 6R martensite

The local 6R structure martensite is not perfect but contains stacking faults (figure 5), extended dislocations (figure 6) and basal plane twins (figure 7). When crossing the stacking fault, the stacking sequence changes from AB′CA′BC′AB′CA′BC′ to AB′CA′BC′BC′AB′CA′, as shown in figure 5. There is one more atomic plane on the upper side of the extended dislocation *PQ* than on the lower side. The proposed model of the extended dislocation with a Burgers vector $\frac{1}{4}[210]_{6R}$ is shown in figure 8 where the

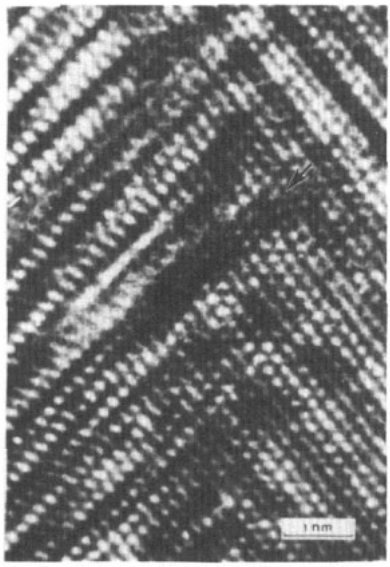

Figure 9. HREM image along the [010] zone axis of the $18R_1$ martensite in step-quenched Cu–17.4 at.% Zn–13.0 at.% Al alloy, showing the (2, 0, 20) twin boundary. The arrow shows an edge dislocation whose Burgers vector has a component **c**/18.

Burgers vector $\boldsymbol{b}_1 = \frac{1}{4}[210] = \frac{1}{12}[230] + \frac{1}{3}[100]$ is dissociated into two partial dislocations with Burgers vectors $\boldsymbol{b}_P = \frac{1}{12}[230]$ and $\boldsymbol{b}_Q = \frac{1}{3}[100]$ respectively. Two Shockley partials P and Q are joined by a stacking fault PQ and the Burgers vector $\boldsymbol{b}_1 = \frac{1}{4}[210]$ is in turn not a lattice translation vector for the ordered martensite. When crossing the basal plane twin TT shown in figure 7, the stacking sequence is reversed as AB′CA′B|C′BA′CB′A where the vertical line (|) across the capital C′ denotes the twin plane.

3.3. Fine structure of the (2, 0, 20)$_{18R_1}$ twin boundary of 18R$_1$ martensite

Figure 9 is a HREM image along the [010] zone axis showing the $(2, 0, 20)_{18R_1}$ twin boundary of $18R_1$ martensite. The left-hand side variant appears misoriented which may arise from the fact that the [010] directions of the two variants are not exactly parallel. A similar phenomenon was observed by Cook *et al* [9] and by Lovey *et al* [12] for the $(12\bar{8})_{18R_1}$ twin boundary. From the corresponding low-magnification HREM image it is evident that the $(2, 0, 20)_{18R_1}$ twin boundary is not planar but curved microscopically. Some segments of the boundary are nearly parallel to the basal plane of the left-hand side variant. Moreover, the coherency of the (2, 0, 20) twin boundary appears much less than that of the $(12\bar{8})$ twin boundary as shown in figure 7(*c*) of [12].

The atomic columns in the neighbourhood of the boundary are displaced from their regular positions. Some $(0, 0, 18)_{18R_1}$ lattice planes on the right-hand side variant are curved near the twin boundary and there even exist some edge dislocations, whose Burgers vector has a component in the [001] direction (see the arrowed region in figure 9).

Acknowledgment

This project was supported by the National Natural Science Foundation of China.

References

[1] Otsuka K and Shimizu K 1986 *Int. Metall. Rev.* **31** 93
[2] Sinclair R and Mohamed H A 1978 *Acta Metall.* **26** 623
[3] Fukumachi M and Kajiwara S 1980 *Japan. J. Appl. Phys.* **19** L479
[4] Knowles K M 1981 *Electron Microscopy and Analysis 1981* (*Inst. Phys. Conf. Ser 61*) ed M J Goringe (Bristol: Institute of Physics) p 413
[5] Knowles K M 1982 *Proc. R. Soc.* A**380** 187
[6] Knowles K M 1982 *Phil. Mag.* A**45** 357
[7] Knowles K M, Christian J W and Smith D A 1982 *J. Physique Coll.* **43** C4 185
[8] Cook J M, Smith D J and Stobbs W M 1981 *Electron Microscopy and Analysis 1981* (*Inst. Phys. Conf. Ser. 61*) ed M J Goringe (Bristol: Institute of Physics) p 417
[9] Cook J M, O'Keefe M A, Smith D J and Stobbs W M 1983 *J. Microsc.* **129** 295
[10] Stobbs W M 1983 *J. Microsc.* **129** 307
[11] Adachi K and Perkins J 1985 *Metall. Trans.* A **16** 1551
[12] Lovey F C, Van Tendeloo G, Van Landuyt J and Amelinckx S 1986 *Proc. Int. Conf. on Martensitic Transformation* (Tokyo: Japan Institute of Metals) p 762
[13] Lovey F C, Van Tendeloo G and Van Languyt J 1987 *Scr. Metall.* **21** 1627
[14] Coene W, Bender H, Lovey F C, Van Dyck D and Amelinckx S 1985 *Phys. Status Solidi* a **87** 483
[15] Tadaki T, Kakeshita T and Shimizu K 1982 *J. Physique Coll.* **43** C4 191
[16] Lovey F C 1987 *Acta Metall.* **35** 1103
[17] Lovey F C, Van Tendeloo G, Van Landuyt J, Delaey L and Amelinckx S 1984 *Phys. Status Solidi* a **86** 553
[18] Lovey F C, Coene W, Van Dyck D, van Tendeloo G, van Landuyt J and Amelinckx S 1984 *Ultramicroscopy* **15** 345
[19] Andrade M, Chandrasekaran M and Delaey L 1984 *Acta Metall.* **32** 1809
[20] Andrade M, Delaey L and Chandrasekaran M 1982 *J. Physique Coll.* **43** C4 673
[21] Saburi T, Inada Y, Nenno S and Hori N 1982 *J. Physique Coll.* **43** C4 633
[22] Wang R, Zhao Y and Gui J 1987 *J. Electron Microsc. Technique* **7** 293
[23] Suzuki T 1981 *Metall. Trans.* A **12** 709